SCIENCE CHINA
Information Sciences

• RESEARCH PAPER •

November 2021, Vol. 64 212302:1–212302:9
https://doi.org/10.1007/s11432-020-2970-y

Self-interference cancellation for cooperative jamming communications with nonideal alignment and channel equalization

Wenbo GUO, Yimin HE, Hongzhi ZHAO*, Shihai SHAO* & Youxi TANG

National Key Laboratory of Science and Technology on Communications, University of Electronic Science and Technology of China, Chengdu 611731*, China*

Received 11 March 2020/Revised 8 May 2020/Accepted 24 June 2020/Published online 13 October 2021

Abstract For the security of wireless communications, cooperative jamming can be used to intentionally degrade the signal-to-noise ratios received by eavesdroppers. Unfortunately, this jamming may also propagate to the legal receiver and then becomes a harmful self-interference (SI), which should be cancelled for reliable detection of the desired signal. In this paper, by comprehensively considering nonideal time-frequency alignment and channel equalization, SI-cancellation capability is investigated for the additive white Gaussian noise channel. Theoretical and simulation results demonstrated that the impact of the frequency alignment error is more serious than that of the time alignment and channel equalization errors. Moreover, it is illustrated that weaker SI power can tolerate a larger range of those nonidealities.

Keywords cooperative jamming, self-interference, time-frequency alignment, channel equalization, nonidealities.

Citation Guo W B, He Y M, Zhao H Z, et al. Self-interference cancellation for cooperative jamming communications with nonideal alignment and channel equalization. Sci China Inf Sci, 2021, 64(11): 212302, https://doi.org/10.1007/s11432-020-2970-y

1 Introduction

Wireless communication becomes more and more popular because of its open nature, making it easily accessible. Unfortunately, this convenience of accessibility can also make it easy to be overheard [1]. Therefore, preventing users' communication information from illegal eavesdroppers to ensure information privacy is the most basic requirement of wireless communication systems. With the development of quantum computers, traditional upper layer methods based on cryptographic encryption and decryption may no longer be secured, making physical layer security recently receiving extensive attention [2]. For instance, Riihonen et al. [3] exploited full-duplex (FD) radios for military jamming, where FD transceivers received the desired signals while transmitting the jamming signals simultaneously, for both defensive and offensive applications. Another promising technique that enhances wireless secrecy via cooperation is cooperative jamming, which can be used for intentionally degrading the signal-to-noise ratios received by eavesdroppers [4]. Moreover, cooperative jamming may also have some potential applications in the coming era of the Internet of Things, where communication networks present a high degree of heterogeneity [5] and wireless devices can cooperate in the jamming to improve network security [6]. For example, with the development of wireless power transfer technologies, energy-harvesting-enabled cooperative jamming is proposed to stimulate low-power idle devices to cooperate in jamming to help ensure the communication secrecy of other actively communicating devices, without increasing the complexity of networks [7].

Although the jamming can confuse the eavesdroppers, it would also be received by the legal receiver and then becomes a harmful self-interference (SI). Fortunately, the legal receiver already knows the original jamming data, making it possible to suppress the SI through SI-cancellation techniques [8]. In recent years, many studies always assume that SI can be removed totally with efficient SI-cancellation

* Corresponding author (email: lyn@uestc.edu.cn, ssh@uestc.edu.cn)

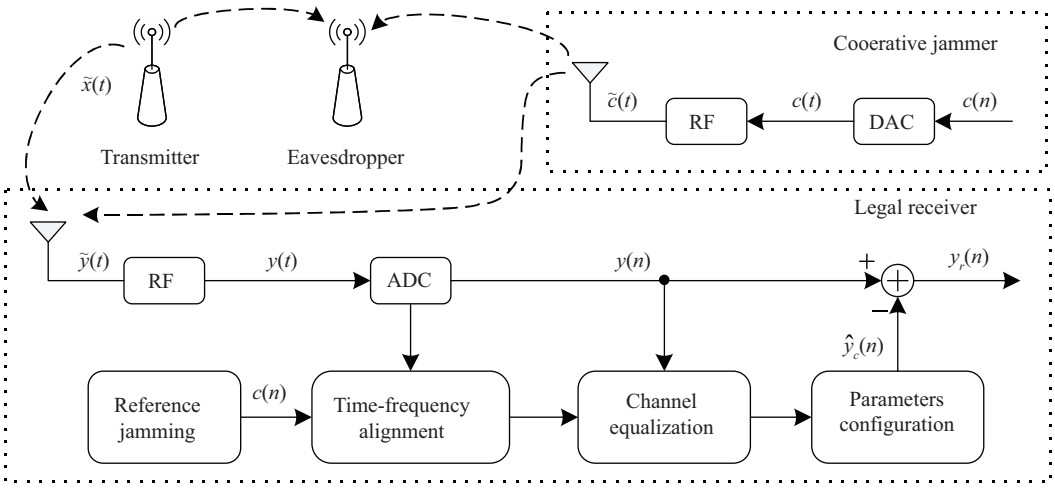

Figure 1 Block diagram of a cooperative jamming system, consisting of a transmitter, a cooperative jammer, a legal receiver, and an eavesdropper.

and thus focus on the optimization of outage probability and secrecy capacity via some power-allocation strategies [9–13]. In fact, because of the propagation channel and the hardware restrictions, the SI may suffer time delay, frequency offset, and unknown channel gain. Generally, perfect time-frequency alignment [14] and channel equalization [15] are always difficult to achieve in practice, making it hard to cancel the SI completely. Furthermore, if the SI is much stronger than the desired signal, a slight time-frequency alignment or channel equalization error may cause a residual SI, degrading the security performance.

For this reason, the impact of channel error on SI-cancellation capability was investigated by He et al. [16], by assuming that the remaining parameters were perfectly estimated and compensated. Similarly, under the assumption of perfect time alignment and channel equalization, the impact of frequency offset on SI-cancellation capability was studied by Guo et al. [17]. Unfortunately, as far as we know, the combined impacts of nonideal time-frequency alignment and channel equalization on SI-cancellation have not been addressed. Motivated by this problem, we derived a closed-form expression of the residual SI power for the additive white Gaussian noise (AWGN) channel, by comprehensively considering the nonideal time-frequency alignment and channel equalization.

The remainder of this paper is outlined as follows: The system model of SI-cancellation with nonideal time-frequency alignment and channel equalization for cooperative jamming systems is presented in Section 2. The combined impacts of time-frequency alignment and channel equalization errors on residual SI power are analyzed in Section 3. Numerical results are discussed in Section 4, and a brief conclusion is summarized in Section 5.

2 System model

A cooperative jamming system is shown in Figure 1, where a transmitter sends the desired signal $\tilde{x}(t)$ to the legal receiver in the presence of an eavesdropper. Simultaneously, a cooperative jammer sends a jamming signal $\tilde{c}(t)$ to intentionally confuse the eavesdropper, and this jamming signal follows a zero-mean Gaussian distribution [18]. Unfortunately, the cooperative jamming would also be received by the legal receiver and becomes a harmful SI.

2.1 Signal reception

Assuming that the desired signal and the SI are independent of each other and both of them are transmitted over the AWGN channel, the total ratio frequency reception at the legal receiver is given by the following equation:

$$\tilde{y}(t) = h_x \tilde{x}(t - \tau_x) + h_c \tilde{c}(t - \tau_c) + \tilde{n}(t), \tag{1}$$

where h_x and h_c represent the complex channel attenuations of the desired signal and the SI, respectively. Additionally, τ_x and τ_c represent the propagation delays from the transmitter to the receiver and from the cooperative jammer to the receiver, respectively.

In addition, $\tilde{x}(t)$ and $\tilde{c}(t)$ respectively denote the desired signal and the cooperative jamming at the transmitting antennas, and they are expressed as follows:

$$\tilde{x}(t) = \sqrt{P_x} x(t) \mathrm{e}^{\mathrm{j}(2\pi f_x t + \varphi_x)}, \tag{2}$$

$$\tilde{c}(t) = \sqrt{P_c} c(t) \mathrm{e}^{\mathrm{j}(2\pi f_c t + \varphi_c)}, \tag{3}$$

where P_x, f_x, and φ_x denote the power, carrier frequency, and initial phase associated with $\tilde{x}(t)$, respectively. Similarly, P_c, f_c, and φ_c denote the power, carrier frequency, and initial phase associated with $\tilde{c}(t)$, respectively. Furthermore, $\tilde{n}(t)$ is the AWGN at the receiver.

Subsequently, $\tilde{y}(t)$ is down-converted by mixing with the local oscillator in the receiver, whose carrier frequency and initial phase are f_y and φ_y, respectively. The obtained baseband signal is given by

$$\begin{aligned} y(t) &= \tilde{y}(t) \mathrm{e}^{-\mathrm{j}(2\pi f_y t + \varphi_y)} \\ &= |h_x| \sqrt{P_x} x(t - \tau_x) \mathrm{e}^{\mathrm{j}(2\pi \Delta f_x t + \Delta\varphi_x)} + |h_c| \sqrt{P_c} c(t - \tau_c) \mathrm{e}^{\mathrm{j}(2\pi \Delta f_c t + \Delta\varphi_c)} + n(t), \end{aligned} \tag{4}$$

where $\Delta f_x = f_x - f_y$ and $\Delta\varphi_x = \varphi_x - \varphi_y - 2\pi f_x \tau_x + \angle h_x$ denote the frequency and phase offsets between the transmitter and the receiver, respectively. Similarly, $\Delta f_c = f_c - f_y$ and $\Delta\varphi_c = \varphi_c - \varphi_y - 2\pi f_c \tau_c + \angle h_c$ denote the frequency and phase offsets between the cooperative jammer and the receiver, respectively. In addition, $|\cdot|$ and $\angle\cdot$ respectively denote the amplitude and phase of the channel attenuation.

Next, $y(t)$ is sampled by the analog-to-digital converter with sampling time T_s, and the obtained digital signal is expressed as

$$\begin{aligned} y(n) &= |h_x| \sqrt{P_x} x(n - D_x) \mathrm{e}^{\mathrm{j}(2\pi F_x n + \Delta\varphi_x)} + |h_c| \sqrt{P_c} c(n - D_c) \mathrm{e}^{\mathrm{j}(2\pi F_c n + \Delta\varphi_c)} + \omega(n) \\ &= y_x(n) + y_c(n) + \omega(n), \end{aligned} \tag{5}$$

where $D_x = \frac{\tau_x}{T_s}$ and $F_x = \Delta f_x T_s$ denote the normalized time delay and the normalized frequency offset between the transmitter and the receiver. Similarly, $D_c = \frac{\tau_c}{T_s}$ and $F_c = \Delta f_c T_s$ denote the normalized time delay and the normalized frequency offset between the cooperative jammer and the receiver.

2.2 SI-cancellation

For implementing effective SI-cancellation, $y_c(n)$ should be accurately estimated and reconstructed from the reference jamming data that has been pre-stored in the legal receiver [19]. Assuming that the estimations of the normalized time delay, the normalized frequency offset, the normalized amplitude attenuation, and the phase shift of the SI are given by

$$\hat{D}_c = D_c + \tau, \tag{6}$$

$$\hat{F}_c = F_c + \varepsilon, \tag{7}$$

$$\left|\hat{h}_c\right| = (1 + \eta) |h_c|, \tag{8}$$

$$\Delta\hat{\varphi}_c = \Delta\varphi_c - 2\pi\varepsilon N \left\lfloor \frac{n}{N} \right\rfloor + \theta, \tag{9}$$

where τ, ε, η, and θ denote the normalized time, frequency, amplitude errors, and phase error, respectively. Furthermore, N represents the estimation period, and based on this, $2\pi\varepsilon N \left\lfloor \frac{n}{N} \right\rfloor$ is the phase shift resulted from the normalized frequency estimation error ε in N symbols, where $\lfloor\cdot\rfloor$ denotes the floor operation. Now, configuring those estimations to the reference jamming, the reconstructed SI can be formulated as

$$\hat{y}_c(n) = \left|\hat{h}_c\right| \sqrt{P_c} c\left(n - \hat{D}_c\right) \mathrm{e}^{\mathrm{j}(2\pi \hat{F}_c n + \Delta\hat{\varphi}_c)} = (1 + \eta) y_c(n - \tau) \mathrm{e}^{\mathrm{j}(2\pi\varepsilon n - 2\pi\varepsilon N \lfloor \frac{n}{N} \rfloor + \theta)}. \tag{10}$$

After subtracting the reconstructed SI $\hat{y}_c(n)$ from the total reception $y(n)$, the residual signal is given as follows:

$$y_r(n) = y(n) - \hat{y}_c(n) = y_x(n) + \Delta y_c(n) + \omega(n), \tag{11}$$

where $\Delta y_c(n) = y_c(n) - \hat{y}_c(n)$ represents the residual SI, which is highly dependent on the accuracies of time-frequency alignment and channel equalization.

3 Impacts of nonideal time-frequency alignment and channel equalization

By comprehensively considering the nonideal time-frequency alignment and channel equalization, the SI-cancellation capability is analyzed in this section.

To begin with, we rewrite (10) as

$$\begin{aligned}\hat{y}_c(n) &= (1+\eta)\, y_c(n-\tau)\, \mathrm{e}^{\mathrm{j}(2\pi\varepsilon n - 2\pi\varepsilon N\lfloor \frac{n}{N}\rfloor + \theta)} \\ &\overset{(a)}{=} (1+\eta)\, h_\tau(0)\, y_c(n)\, \mathrm{e}^{\mathrm{j}(2\pi\varepsilon n - 2\pi\varepsilon N\lfloor \frac{n}{N}\rfloor + \theta)} + \hat{y}_c^{\tau}(n),\end{aligned} \tag{12}$$

where (a) holds by using [17]

$$y_c(n-\tau) = \sum_{i=-\infty}^{+\infty} y_c(n-i)\, h_\tau(i), \tag{13}$$

$$h_\tau(n) = \frac{\sin[\pi(n-\tau)]}{\pi(n-\tau)}. \tag{14}$$

Besides, we denote

$$\hat{y}_c^{\tau}(n) = (1+\eta)\, \mathrm{e}^{\mathrm{j}\left(2\pi\varepsilon n - 2\pi\varepsilon N\lfloor \frac{n}{N}\rfloor + \theta\right)} \sum_{\substack{i=-\infty \\ i\neq 0}}^{+\infty} y_c(n-i)\, h_\tau(i). \tag{15}$$

After N-point discrete Fourier transform (DFT), Eq. (12) can be expressed as

$$\begin{aligned}\hat{Y}_c(k) &= \sum_{n=0}^{N-1} \hat{y}_c(n)\, \mathrm{e}^{-\mathrm{j}\frac{2\pi}{N}nk} \\ &= (1+\eta)\, h_\tau(0)\, \mathrm{e}^{\mathrm{j}\theta} \sum_{n=0}^{N-1} y_c(n) \mathrm{e}^{-\mathrm{j}\frac{2\pi}{N}n(k-N\varepsilon)} + \hat{Y}_c^{\tau}(k) \\ &= (1+\eta)\, h_\tau(0)\, \mathrm{e}^{\mathrm{j}\theta} Y_c(k-N\varepsilon) + \hat{Y}_c^{\tau}(k),\end{aligned} \tag{16}$$

where

$$Y_c(k) = \sum_{n=0}^{N-1} y_c(n)\, \mathrm{e}^{-\mathrm{j}\frac{2\pi}{N}nk}, \tag{17}$$

$$\hat{Y}_c^{\tau}(k) = \sum_{n=0}^{N-1} \hat{y}_c^{\tau}(n)\, \mathrm{e}^{-\mathrm{j}\frac{2\pi}{N}nk} \tag{18}$$

denote the N-point DFT of $y_c(n)$ and $\hat{y}_c^{\tau}(n)$, respectively.

Similar to (13), we can further express (16) as

$$\hat{Y}_c(k) = (1+\eta)\, h_\tau(0)\, h_\varepsilon(0)\, \mathrm{e}^{\mathrm{j}\theta} Y_c(k) + \hat{Y}_c^{\varepsilon}(k) + \hat{Y}_c^{\tau}(k), \tag{19}$$

where

$$\hat{Y}_c^{\varepsilon}(k) = (1+\eta)\, h_\tau(0)\, \mathrm{e}^{\mathrm{j}\theta} \sum_{\substack{i=-\infty \\ i\neq 0}}^{+\infty} h_\varepsilon(i)\, Y_c(k-i), \tag{20}$$

$$h_\varepsilon(k) = \frac{\sin[\pi(k-N\varepsilon)]}{\pi(k-N\varepsilon)}. \tag{21}$$

Applying N-point inverse discrete Fourier transform (IDFT) to (19), the reconstructed SI can be reformulated as

$$\hat{y}_c(n) = \frac{1}{N}\sum_{k=0}^{N-1} \hat{Y}_c(k)\, \mathrm{e}^{\mathrm{j}\frac{2\pi}{N}nk} = (1+\eta)\, h_\tau(0)\, h_\varepsilon(0)\, \mathrm{e}^{\mathrm{j}\theta} y_c(n) + \hat{y}_c^{\varepsilon}(n) + \hat{y}_c^{\tau}(n). \tag{22}$$

Then, the residual SI can be expressed as

$$\Delta y_c(n) = y_c(n) - \hat{y}_c(n) = \left[1 - (1+\eta) h_\tau(0) h_\varepsilon(0) \mathrm{e}^{\mathrm{j}\theta}\right] y_c(n) - \hat{y}_c^{\varepsilon}(n) - \hat{y}_c^{\tau}(n). \tag{23}$$

According to (15) and (20), it obtains that $\hat{y}_c^{\tau}(n)$ and $\hat{y}_c^{\varepsilon}(n)$ are the linear combinations of the delayed duplicates of $y_c(n)$, leading that $\hat{y}_c^{\tau}(n)$ and $\hat{y}_c^{\varepsilon}(n)$ follow the Gaussian distributions and are uncorrelated with $y_c(n)$ owing to the Gaussian characteristic of the SI. Thus, the residual SI follows the Gaussian distribution, which confirms the correctness that the residual SI is designed as Gaussian distribution in many literatures [20–22].

Therefore, the power of the residual SI can be calculated as

$$\begin{aligned}\mathrm{P}\{\Delta y_c(n)\} &= \left|1 - (1+\eta) h_\tau(0) h_\varepsilon(0) \mathrm{e}^{\mathrm{j}\theta}\right|^2 |h_c|^2 P_c + \mathrm{P}\left\{\hat{y}_c^{\varepsilon}(n) + \hat{y}_c^{\tau}(n)\right\} \\ &= \left[1 - 2(1+\eta) h_\tau(0) h_\varepsilon(0) \cos\theta + (1+\eta)^2 h_\tau^2(0) h_\varepsilon^2(0)\right] |h_c|^2 P_c + \mathrm{P}\left\{\hat{y}_c^{\varepsilon}(n) + \hat{y}_c^{\tau}(n)\right\}.\end{aligned} \tag{24}$$

Combining (22), $\mathrm{P}\left\{\hat{y}_c^{\varepsilon}(n) + \hat{y}_c^{\tau}(n)\right\}$ can be calculated as

$$\begin{aligned}\mathrm{P}\left\{\hat{y}_c^{\varepsilon}(n) + \hat{y}_c^{\tau}(n)\right\} &= \mathrm{P}\left\{\hat{y}_c(n)\right\} - \left|(1+\eta) h_\tau(0) h_\varepsilon(0) \mathrm{e}^{\mathrm{j}\theta}\right|^2 |h_c|^2 P_c \\ &= (1+\eta)^2 \left[1 - h_\tau^2(0) h_\varepsilon^2(0)\right] |h_c|^2 P_c,\end{aligned} \tag{25}$$

because $\mathrm{P}\left\{\hat{y}_c(n)\right\} = (1+\eta)^2 |h_c|^2 P_c$.

Substituting (25) into (24), the power of the residual SI can be calculated in dB as

$$\Delta P = 10\lg \mathrm{P}\left\{\Delta y_c(n)\right\} = P + 10\lg\alpha, \tag{26}$$

where $P = 10\lg|h_c|^2 P_c$ denotes the received SI power at the receiver, and α denotes the cancellation factor, and can be expressed as

$$\alpha = \eta^2 + 2(1+\eta)\left[1 - \frac{\sin(\pi N\varepsilon)\sin(\pi\tau)\cos\theta}{\pi^2 N\varepsilon\tau}\right]. \tag{27}$$

From (26) and (27), we can observe the following conclusions.

(1) With ideal time-frequency alignment and channel equalization, the residual SI power is calculated as

$$\Delta P_\infty = 10\lg 0 = -\infty. \tag{28}$$

(2) With ideal frequency alignment and channel equalization, the residual SI power is approximated in two cases.

Case 1. For $\tau \leqslant 1$, we have

$$\Delta P_\tau = 10\lg 2\left[1 - \frac{\sin(\pi\tau)}{\pi\tau}\right] + P \overset{(\mathrm{b}_\tau)}{\approx} 10\lg\frac{\pi^2}{3}\tau^2 + P = 20\lg\tau + 10\lg\frac{\pi^2}{3} + P, \tag{29}$$

where (b_τ) holds by using $\sin(x) \approx x - \frac{x^3}{6}$.

Case 2. For $\tau > 1$, we have

$$\Delta P_\tau = 10\lg 2\left[1 - \frac{\sin(\pi\tau)}{\pi\tau}\right] + P \approx P + 3. \tag{30}$$

(3) With ideal time alignment and channel equalization, the residual SI power is approximated in two cases.

Case 1. For $\varepsilon \leqslant \frac{1}{N}$, we have

$$\Delta P_\varepsilon = 10\lg 2\left[1 - \frac{\sin(\pi N\varepsilon)}{\pi N\varepsilon}\right] + P \overset{(\mathrm{b}_\varepsilon)}{\approx} 10\lg\frac{\pi^2 N^2}{3}\varepsilon^2 + P = 20\lg\varepsilon + 10\lg\frac{\pi^2 N^2}{3} + P, \tag{31}$$

where (b_ε) holds by using $\sin(x) \approx x - \frac{x^3}{6}$.

Case 2. For $\varepsilon > \frac{1}{N}$, we have

$$\Delta P_\tau = 10\lg 2\left[1 - \frac{\sin(\pi N\varepsilon)}{\pi N\varepsilon}\right] + P \approx P + 3. \tag{32}$$

(4) With ideal time-frequency alignment and phase equalization, the residual SI power is simplified as

$$\Delta P_\eta = 10\lg \eta^2 + P = 20\lg \eta + P. \tag{33}$$

(5) With ideal time-frequency alignment and amplitude equalization, for $\theta \leqslant 1$ rad, the residual SI power is approximated as

$$\Delta P_\theta = 10\lg 2(1-\cos\theta) + P \overset{(\mathrm{b}_\theta)}{\approx} 10\lg \theta^2 + P = 20\lg\theta + P, \tag{34}$$

where (b_θ) holds by using $\cos(x) \approx 1 - \frac{x^2}{2}$.

Specifically, when $\theta = \pi$ rad, the residual SI power is approximated as

$$\Delta P_\theta = 10\lg 2(1-\cos\theta) + P \approx P + 6. \tag{35}$$

4 Simulation results

Simulation of the results was conducted to validate the theoretical analysis. In the simulations made, the transmitter sent a quadrature phase shift keying (QPSK) signal to the receiver. Concurrently, the cooperative jammer sent a jamming signal with zero-mean Gaussian characteristics. The carrier frequency was set as $f_c = 2.4$ GHz, the signal bandwidth was set as $B = 10$ MHz, and the analog-to-digital converter (ADC) sampling time was set as $T_s = 0.1$ μs. Unless otherwise specified, it was assumed that the parameter estimation period was $N = 1024$ symbols. In addition, by assuming a noise factor of 4 dB, the noise floor was set at -100 dBm.

Figure 2 displays the impact of the normalized time alignment error on ΔP regardless of the frequency, amplitude, and phase errors. As we can see, the simulation results match the theoretical curves obtained from (26) and (27) for arbitrary τ ranging from 10^{-4} to 10^{1}. In addition, the residual SI power ΔP is proportional to $\lg\tau$ for $\tau \leqslant 1$, which is similar to that in (29). Besides, when $\tau > 1$, the residual SI power ΔP converges to the received SI power P plus 3 dB, which is similar with that in (30). This indicates that when the time error exceeds one symbol, the time alignment between the reconstructed SI and the received SI failed to implement. Therefore, the reconstructed SI would almost be uncorrelated to the received SI, causing the residual SI power to double.

The impact of the normalized frequency alignment error on ΔP regardless of the time, amplitude, and phase errors is illustrated in Figure 3. It is shown that the simulation results are similar with the theoretical curves obtained from (26) and (27) for arbitrary ε ranging from 10^{-7} to 10^{-2}. When $\varepsilon \leqslant 10^{-3}$, the residual SI power ΔP is proportional to $\lg\varepsilon$, which is coincident with that in (31). Besides, when $\varepsilon > 10^{-3}$, the residual SI power converges to the received SI power P plus 3 dB, which is similar with that in (32). This indicates that when the frequency error is greater than $\frac{1}{N}$ of the bandwidth, the reconstructed SI would almost be uncorrelated to the received SI, causing the residual SI power to double.

The impact of the normalized amplitude equalization error on ΔP regardless of the time, frequency, and phase errors is depicted in Figure 4. One can see that the simulation results agree with the theoretical curves drawn from (26) and (27) for arbitrary η ranging from 10^{-4} to 10^{0}. It is obvious that the residual SI power ΔP is proportional to $\lg\eta$, which is similar to the analysis of (33).

Figure 5 shows the impact of phase equalization error on ΔP regardless of the time, frequency, and amplitude error. As can be seen, the simulation results are consistent with the theoretical curves drawn from (26) and (27) for arbitrary θ ranging from 10^{-4} rad to 10^{1} rad. When $\theta \leqslant 10^{0}$ rad, the residual SI power ΔP is proportional to $\lg\theta$, which is similar with that in (34). Besides, for $\theta > 10^{0}$ rad, as the phase error increases, the residual SI power ΔP first increases and then decreases. The maximum ΔP is the received SI power P plus 6 dB, and its corresponding phase error is reached at π rad, indicating that the phase of the reconstructed SI is opposite to the phase of the received SI, which agrees with the analysis of (35).

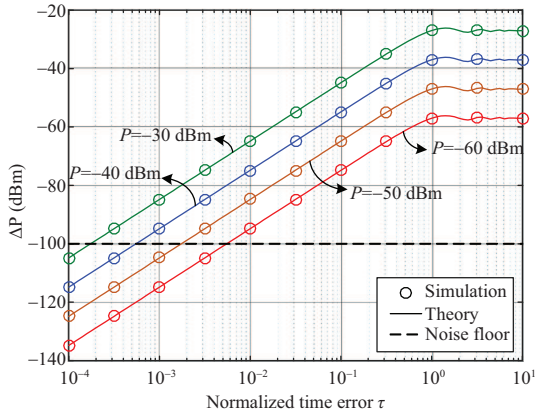

Figure 2 (Color online) Impact of the normalized time alignment error on ΔP, where the received SI power P is set as -30 dBm, -40 dBm, -50 dBm, and -60 dBm.

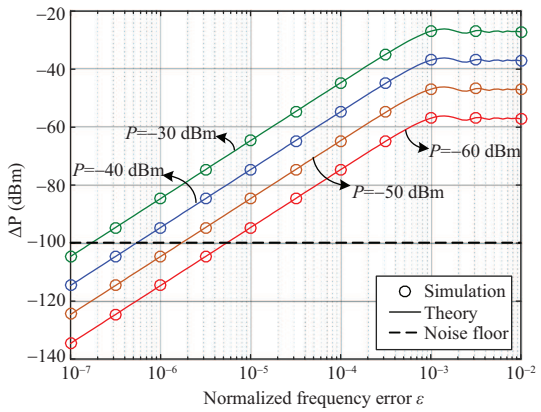

Figure 3 (Color online) Impact of the normalized frequency alignment error on ΔP, where the received SI power P is set as -30 dBm, -40 dBm, -50 dBm, and -60 dBm.

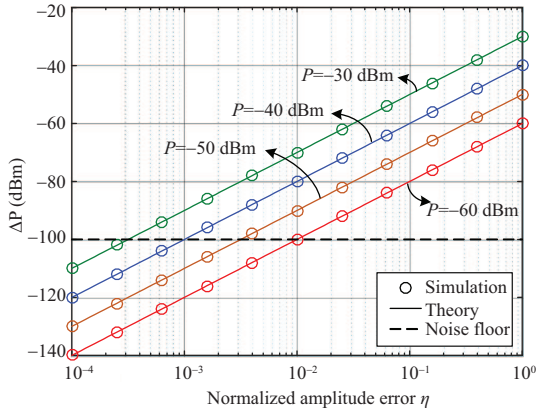

Figure 4 (Color online) Impact of the normalized amplitude equalization error on ΔP, where the received SI power P is set as -30 dBm, -40 dBm, -50 dBm, and -60 dBm.

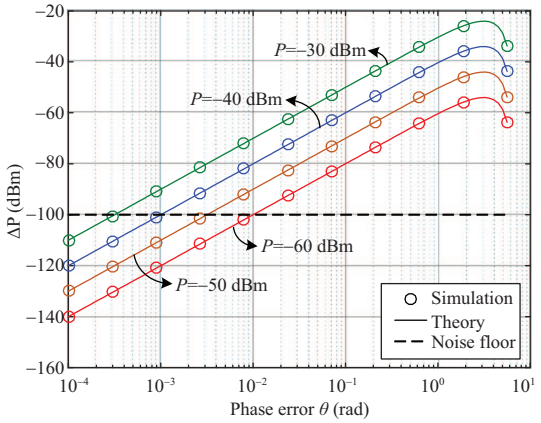

Figure 5 (Color online) Impact of the normalized phase equalization error on ΔP, where the received SI power P is set as -30 dBm, -40 dBm, -50 dBm, and -60 dBm.

Table 1 Time-frequency alignment and channel equalization errors

Parameter errors	τ	ε	η	θ (rad)
Condition 1	10^{-4}	10^{-3}	10^{-2}	10^{-1}
Condition 2	10^{-7}	10^{-6}	10^{-5}	10^{-4}
Condition 3	10^{-4}	10^{-3}	10^{-2}	10^{-1}
Condition 4	10^{-4}	10^{-3}	10^{-2}	10^{-1}

From Figures 2–5, it is observed that the residual SI power is more sensitive to frequency error compared to the time alignment and channel equalization errors. Furthermore, the residual SI power increases with the received SI power, providing lower acceptable alignment and channel errors. For instance, when the received SI power is $P = -60$ dBm, to ensure that the residual SI below the noise floor, the normalized time error should be less than 5×10^{-3}, the normalized frequency error should be less than 5×10^{-6}, the normalized amplitude error should be less than 1×10^{-2}, and the phase error should be less than 1×10^{-2} rad. However, when the received SI power is $P = -30$ dBm, to ensure that the residual SI is below the noise floor, the normalized time error should be less than 2×10^{-4}, the normalized frequency error should be less than 2×10^{-7}, the normalized amplitude error should be less than 3×10^{-4}, and the phase error should be less than 3×10^{-4} rad.

With different time-frequency alignment and channel estimation errors, as shown in Table 1, Figure 6 gives the relationship between the residual SI power ΔP and the received SI power P. It is observed that the simulation results match the theoretical curves drawn from (26) and (27) for all conditions, and the

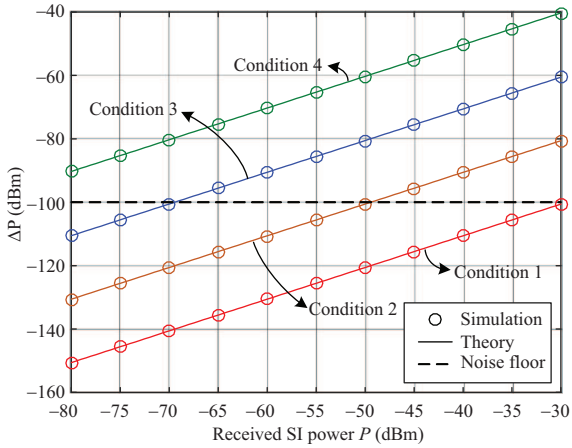

Figure 6 (Color online) Relationship between the residual SI power and the received SI power with different time-frequency alignment and channel equalization errors.

residual SI power is proportional to the received SI power. Furthermore, for the same received SI power, as the time-frequency alignment and channel equalization errors increase, the residual SI power increases.

5 Conclusion

This paper investigated SI-cancellation capability in cooperative jamming communication systems, by jointly considering nonideal time-frequency alignment and channel equalization. For the AWGN channel, an exact closed-form expression of the residual SI power was derived. Simulation results confirmed that system performance was more sensitive to the nonideal frequency alignment compared to the nonideal time alignment and nonideal channel equalization. Moreover, weaker SI power can tolerate a larger range of nonidealities. The contributions can provide guidance for designing practical SI-cancellation in cooperative jamming communications.

Acknowledgements This work was supported by National Key Research and Development Program of China (Grant No. 2018YFB1801903), National Natural Science Foundation of China (Grant Nos. 61771107, 61701075, 61601064, 61531009), and Sichuan Science and Technology Program (Grant No. 2019JDRC0006).

References

1 Goel S, Negi R. Guaranteeing secrecy using artificial noise. IEEE Trans Wirel Commun, 2008, 7: 2180–2189
2 Wang H M, Xia X G. Enhancing wireless secrecy via cooperation: signal design and optimization. IEEE Commun Mag, 2015, 53: 47–53
3 Riihonen T, Korpi D, Rantula O, et al. Inband full-duplex radio transceivers: a paradigm shift in tactical communications and electronic warfare? IEEE Commun Mag, 2017, 55: 30–36
4 Guo W, Zhao H, Tang Y. Testbed for cooperative jamming cancellation in physical layer security. IEEE Wirel Commun Lett, 2020, 9: 240–243
5 Du Q, Song H, Zhu X. Social-feature enabled communications among devices toward the smart IoT community. IEEE Commun Mag, 2019, 57: 130–137
6 Lee K, Hong J P, Choi H H, et al. Adaptive wireless-powered relaying schemes with cooperative jamming for two-hop secure communication. IEEE Internet Things J, 2018, 5: 2793–2803
7 Zhang G, Xu J, Wu Q, et al. Wireless powered cooperative jamming for secure OFDM system. IEEE Trans Veh Technol, 2018, 67: 1331–1346
8 Li C, Liu Y, Xu Q, et al. Self-interference cancellation with frequency offset and nonlinear distortion suppression for cooperative jamming communications. IEEE Commun Lett, 2019, 23: 2091–2094
9 Luo M, Wang H M, Yin Q Y. Hybrid relaying and jamming for wireless physical layer security based on cooperative beamforming. Sci Sin Inform, 2013, 43: 445–458
10 Deng H, Wang H M, Wang W J. Grouping cooperative jamming for wireless physical layer security. Sci Sin Inform, 2014, 44: 1482–1494
11 Tang L, Li Q. Wireless power transfer and cooperative jamming for secrecy throughput maximization. IEEE Wirel Commun Lett, 2016, 5: 556–559
12 Wang C L, Cho T N, Liu F. Power allocation and jammer selection of a cooperative jamming strategy for physical-layer security. In: Proceedings of IEEE Vehicular Technology Conference (VTC Spring), Seoul, 2014. 1–5
13 Sarikaya Y, Ercetin O, Gurbuz O. Dynamic control for cooperative jamming with a non-altruistic node. In: Proceedings of IEEE Conference on Communications and Network Security (CNS), National Harbor, 2013. 381–382
14 Zhong S, Xia W, He Z. Joint estimation of time delay and clock error in the incoherent reception systems. Circ Syst Signal Process, 2016, 35: 3284–3309
15 Gao F F, Zhang R, Liang Y C. Optimal channel estimation and training design for two-way relay networks. IEEE Trans Commun, 2009, 57: 3024–3033

16 He Z, Shao S, Shen Y, et al. Performance analysis of RF self-interference cancellation in full-duplex wireless communications. IEEE Wirel Commun Lett, 2014, 3: 405–408
17 Guo W, Zhao H, Ma W, et al. Effect of frequency offset on cooperative jamming cancellation in physical layer security. In: Proceedings of IEEE Globecom Workshops (GC Wkshps), Abu Dhabi, 2018. 1–5
18 Zheng G, Choo L C, Wong K K. Optimal cooperative jamming to enhance physical layer security using relays. IEEE Trans Signal Process, 2011, 59: 1317–1322
19 Xing H, Liu L, Zhang R. Secrecy wireless information and power transfer in fading wiretap channel. IEEE Trans Veh Technol, 2016, 65: 180–190
20 Duarte M, Dick C, Sabharwal A. Experiment-driven characterization of full-duplex wireless systems. IEEE Trans Wirel Commun, 2012, 11: 4296–4307
21 Zlatanov N, Sippel E, Jamali V, et al. Capacity of the Gaussian two-hop full-duplex relay channel with residual self-interference. IEEE Trans Commun, 2017, 65: 1005–1021
22 Cirik A C, Wang R, Hua Y, et al. Weighted sum-rate maximization for full-duplex MIMO interference channels. IEEE Trans Commun, 2015, 63: 801–815